

Dirac-Brueckner-Hartree-Fock *versus* chiral effective field theory

Francesca Sammarruca,¹ B. Chen,¹ L. Coraggio,² N. Itaco,^{3,2} and R. Machleidt¹

¹ *Physics Department, University of Idaho, Moscow, ID 83844-0903, U.S.A*

² *Istituto Nazionale di Fisica Nucleare,*

Complesso Universitario di Monte S. Angelo, Via Cintia - I-80126 Napoli, Italy

³ *Dipartimento di Scienze Fisiche, Università di Napoli Federico II,*

Complesso Universitario di Monte S. Angelo, Via Cintia - I-80126 Napoli, Italy

(Dated: September 25, 2012)

We compare nuclear and neutron matter predictions based on two different *ab initio* approaches to nuclear forces and the nuclear many-body problem. The first consists of a realistic meson-theoretic nucleon-nucleon potential together with the relativistic counterpart of the Brueckner-Hartree-Fock theory of nuclear matter. The second is based on chiral effective field theory, with density-dependent interactions derived from leading order chiral three-nucleon forces. We find the results to be very close and conclude that both approaches contain important features governing the physics of nuclear and neutron matter.

I. INTRODUCTION

Nuclear matter is a convenient laboratory to test nuclear forces and many body theories. In particular, the equation of state (EoS) of extremely neutron-rich matter has attracted considerable attention lately because of its broad applications, ranging from the structure of rare isotopes to the properties of neutron stars.

Constraints on the properties of nuclear matter, symmetric or isospin-asymmetric, can be obtained from a variety of experiments, such as measurements of nuclear binding energies (including isobaric analog state energies), parity-violating electron scattering, neutron skin thickness measurements, nucleus-nucleus collisions, and astrophysical observations. For a recent review of available constraints, particularly on the nuclear symmetry energy, the reader is referred to Ref. [1].

Diverse theoretical frameworks have been employed to describe the properties of nuclear and neutron matter. They include: phenomenological approaches, both relativistic and non-relativistic; the Brueckner-Hartree-Fock (BHF) method, typically implemented with three-nucleon forces (3NF); variational approaches; the relativistic Dirac-Brueckner-Hartree-Fock (DBHF) approach; and chiral effective field theories. Predictions are model-dependent, particularly at the higher densities, where constraints are scarce and less stringent.

In our previous work with both symmetric nuclear matter (SNM) and isospin-asymmetric nuclear matter (IANM), we have relied on the DBHF approach, together with a relativistic meson-theoretic nucleon-nucleon (NN) potential which uses the pseudovector coupling for the pion [2]. The latter choice was motivated by the considerations we outline next. Already when QCD (and its approximate symmetries) were unknown, it was observed that the contribution from the nucleon-antinucleon pair diagram, Fig. 1, becomes unreasonably large if the pseudoscalar (ps) coupling is used for the pion, leading to very large pion-nucleon scattering lengths [3, 4]. We recall that the Lagrangian density for pseudoscalar coupling of the nucleon field (ψ) with a pseudoscalar meson field (ϕ) is

$$\mathcal{L}_{ps} = -ig_{ps}\bar{\psi}\gamma_5\psi\phi. \quad (1)$$

On the other hand, the same contribution shown in Fig. 1, is heavily suppressed when the pseudovector (pv) coupling is used instead (a mechanism which became known as “pair suppression”). The reason for the suppression is that the covariant derivative in the pseudovector Lagrangian,

$$\mathcal{L}_{pv} = -\frac{f_{ps}}{m_{ps}}\bar{\psi}\gamma_5\gamma^\mu\psi\partial_\mu\phi, \quad (2)$$

generates a vertex that is proportional to momentum (leading to a weak coupling for low momenta) and, thus, explains the small value of the pion-nucleon scattering length at threshold. Non-linear realizations of chiral symmetry [3] can further motivate a preference for the pseudovector coupling.

Back to the many-body problem, the main strength of the DBHF approach is its inherent ability to account for important three-body forces through its density dependence. In Fig. 2 we show a three-body force originating from virtual excitation of a nucleon-antinucleon pair, known as “Z-graph”. Notice that the observations from the previous paragraph ensure that this diagram, as well as the corresponding diagram at the two-body level, Fig. 1, is moderate in size when the pv coupling, Eq. (2), is used. (Hence, the importance of using pv potentials in relativistic nuclear structure calculations.) The main feature of the DBHF method turns out to be closely related to the 3NF depicted

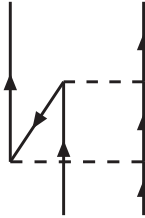


FIG. 1: Contribution to the NN interaction from virtual pair excitation. Upward- and downward-pointing arrows represent nucleons and antinucleons, respectively. Dashed lines denote mesons.

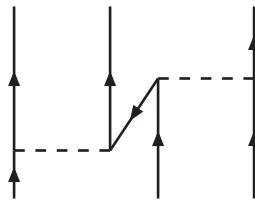


FIG. 2: Three-body force due to virtual pair excitation. Notation as in the previous figure.

in Fig. 2, as we will argue next. In the DBHF approach, one describes the positive energy solutions of the Dirac equation in the medium as

$$u^*(p, \lambda) = \left(\frac{E_p^* + m^*}{2m^*} \right)^{1/2} \begin{pmatrix} \mathbf{1} \\ \frac{\boldsymbol{\sigma} \cdot \mathbf{p}}{E_p^* + m^*} \end{pmatrix} \chi_\lambda, \quad (3)$$

where the nucleon effective mass, m^* , is defined as $m^* = m + U_S$, with U_S an attractive scalar potential. (This will be derived below.) It can be shown that both the description of a single-nucleon via Eq. (3) and the evaluation of the Z-diagram, Fig. 2, generate a repulsive effect on the energy/particle in symmetric nuclear matter which depends on the density approximately as

$$\Delta E \propto \left(\frac{\rho}{\rho_0} \right)^{8/3}, \quad (4)$$

and provides the saturating mechanism missing from conventional Brueckner calculations.

The approximate equivalence of the effective-mass description of Dirac states and the contribution from the Z-diagram has a simple intuitive explanation in the observation that Eq. (3), like any other solution of the Dirac equation, can be written as a superposition of positive and negative energy solutions using free nucleon masses. On the other hand, the “nucleon” in the middle of the Z-diagram, Fig. 2, is precisely a superposition of positive and negative energy states. In summary, the DBHF method effectively takes into account a particular class of 3NF, which are crucial for nuclear matter saturation.

The conventional BHF theory, together with meson-exchange 3NF, can also describe the saturation of nuclear matter in a satisfactory manner, although consistency between the parameters of the two- and the three-body forces can be problematic [5].

Ideally, one wishes to derive nuclear forces from the fundamental theory of strong interactions, QCD. Such task is however not feasible, due to the non-perturbative nature of the theory in the low-energy regime typical of nuclear physics. An alternative way is to respect the symmetries of the QCD Lagrangian while retaining the traditional degrees of freedom relevant to nuclear physics, namely nucleons and pions [6]. This is the philosophy of chiral effective field theory (EFT), which has become popular in recent years.

Effective field theories allow for a systematic expansion in powers of the momentum (or the pion mass) known as chiral perturbation theory (ChPT) such that, at any order, the irreducible two- and many-body diagrams to be included are precisely defined. An extensive review on the subject, including a comprehensive list of references, can be found in Ref. [7].

Chiral EFT has validity only up to the chiral symmetry breaking scale of $\Lambda_\chi \approx 1$ GeV. Thus, the low-momentum expansion has a limited range of applicability. This is another reason why relativistic meson theory has been considered more suitable for applications to dense systems, where high momenta are involved due to the high Fermi momenta. To remedy this problem, ways to extend EFT predictions to higher densities are employed, such as parametrizing the available predictions with accurate fitting functions which are then used to predict the properties of dense astrophysical systems.

It is the purpose of this paper to conduct a comparison between nuclear and neutron matter (NM) predictions obtained with two *ab-initio* approaches:

1. The DBHF method as briefly outlined above, using the Bonn B meson-exchange potential [8].
2. A quantitative chiral NN potential, for which we choose the Idaho N³LO potential of Ref. [9] together with chiral three-nucleon forces at N²LO. Details are given in the next section.

We would like to explore how the DBHF phenomenology compares with the predictions of chiral EFT at N³LO plus leading 3NF, in both symmetric and neutron matter.

We will start with a comparison at the two-body force level. The meson-exchange side of this part of the comparison will be represented by the conventional BHF model. In the meson-exchange sector, realistic saturation properties will be generated through the DBHF model, whereas, on the chiral side, the contribution from leading 3NF will be included. We wish to compare the size and density dependence of the saturating effects in each scheme. We will compare predictions of the equation of state and the symmetry energy in both cases. Neutron star masses and radii will also be addressed.

This paper is organized as follows: In Section II, we review the main points of the DBHF calculation leading to the energy per particle in nuclear matter with arbitrary degree of isospin asymmetry. A brief outline of chiral two- and three-nucleon forces is contained in Section III. Our findings and conclusions are presented in Sections IV and V, respectively.

II. RELATIVISTIC MESON-EXCHANGE POTENTIAL AND DBHF APPROACH

As stated in the Introduction, the starting point of our many-body calculation is a realistic NN interaction which is then applied in the nuclear medium without any additional free parameters.

Relativistic meson theory is an appropriate framework to deal with the high momenta encountered in dense matter. In particular, the one-boson-exchange (OBE) model has proven very successful in describing NN data in free space up to high energy and has a good theoretical foundation. The OBE potential is defined as a sum of one-particle-exchange amplitudes of certain bosons with given mass and coupling. In general, six non-strange bosons with masses below 1 GeV/ c^2 are used. Thus,

$$v = \sum_{\alpha=\pi,\eta,\rho,\omega,\delta,\sigma} v_\alpha^{OBE}, \quad (5)$$

with π and η pseudoscalar, σ and δ scalar, and ρ and ω vector particles. For more details, see Ref. [8].

Among the many available OBE potentials, some being part of the “high-precision generation” [10, 11], we seek a momentum-space potential developed within a relativistic scattering equation, such as the one obtained through the Thompson [12] three-dimensional reduction of the Bethe-Salpeter equation [13].

Having summarized in the Introduction the main DBHF philosophy, for completeness we now proceed to review the main aspects of our approach and the various approximations we perform through the application of the DBHF procedure. The equations we present are those suitable for isospin-asymmetric nuclear matter (IANM), since they naturally contain both the cases of SNM and NM.

We start from the Thompson [12] relativistic three-dimensional reduction of the Bethe-Salpeter equation [13]. The Thompson equation is applied to nuclear matter in strict analogy to free-space scattering and reads, in the nuclear matter rest frame,

$$g_{ij}(\vec{q}', \vec{q}, \vec{P}, (\epsilon_{ij}^*)_0) = v_{ij}^*(\vec{q}', \vec{q}) + \int \frac{d^3K}{(2\pi)^3} v_{ij}^*(\vec{q}', \vec{K}) \frac{m_i^* m_j^*}{E_i^* E_j^*} \frac{Q_{ij}(\vec{K}, \vec{P})}{(\epsilon_{ij}^*)_0 - \epsilon_{ij}^*(\vec{P}, \vec{K})} g_{ij}(\vec{K}, \vec{q}, \vec{P}, (\epsilon_{ij}^*)_0), \quad (6)$$

where g_{ij} is the in-medium reaction matrix ($ij=nn$, pp , or np), and the asterisk signifies that medium effects are applied to those quantities. Thus the NN potential, v_{ij}^* , is constructed in terms of effective Dirac states (in-medium

spinors) as explained above. In Eq. (6), \vec{q} , \vec{q}' , and \vec{K} are the initial, final, and intermediate relative momenta, and $E_i^* = \sqrt{(m_i^*)^2 + K^2}$. The momenta of the two interacting particles in the nuclear matter rest frame have been expressed in terms of their relative momentum and the center-of-mass momentum, \vec{P} , through

$$\vec{P} = \vec{k}_1 + \vec{k}_2 \quad (7)$$

and

$$\vec{K} = \frac{\vec{k}_1 - \vec{k}_2}{2}. \quad (8)$$

The energy of the two-particle system is

$$\epsilon_{ij}^*(\vec{P}, \vec{K}) = e_i^*(\vec{P}, \vec{K}) + e_j^*(\vec{P}, \vec{K}) \quad (9)$$

and $(\epsilon_{ij}^*)_0$ is the starting energy. The single-particle energy e_i^* includes kinetic energy and potential energy contributions (see Eq. (23) below). The Pauli operator, Q_{ij} , prevents scattering to occupied nn , pp , or np states. To eliminate the angular dependence from the kernel of Eq. (6), it is customary to replace the exact Pauli operator with its angle-average. Detailed expressions for the Pauli operator and the average center-of-mass momentum in the case of two different Fermi seas can be found in Ref. [14].

With the definitions

$$G_{ij} = \frac{m_i^*}{E_i^*(\vec{q}')} g_{ij} \frac{m_j^*}{E_j^*(\vec{q})} \quad (10)$$

and

$$V_{ij}^* = \frac{m_i^*}{E_i^*(\vec{q}')} v_{ij}^* \frac{m_j^*}{E_j^*(\vec{q})}, \quad (11)$$

one can rewrite Eq. (6) as

$$\begin{aligned} G_{ij}(\vec{q}', \vec{q}, \vec{P}, (\epsilon_{ij}^*)_0) &= V_{ij}^*(\vec{q}', \vec{q}) \\ &+ \int \frac{d^3 K}{(2\pi)^3} V_{ij}^*(\vec{q}', \vec{K}) \frac{Q_{ij}(\vec{K}, \vec{P})}{(\epsilon_{ij}^*)_0 - \epsilon_{ij}^*(\vec{P}, \vec{K})} G_{ij}(\vec{K}, \vec{q}, \vec{P}, (\epsilon_{ij}^*)_0), \end{aligned} \quad (12)$$

which is formally identical to its non-relativistic counterpart.

The goal is to determine self-consistently the nuclear matter single-particle potential which, in IANM, will be different for neutrons and protons. To facilitate the description of the procedure, we will use a schematic notation for the neutron/proton potential. We write, for neutrons,

$$U_n = U_{np} + U_{nn}, \quad (13)$$

and for protons

$$U_p = U_{pn} + U_{pp}, \quad (14)$$

where each of the four pieces on the right-hand-side of Eqs. (13-14) signifies an integral of the appropriate G -matrix elements (nn , pp , or np) obtained from Eq. (12). Clearly, the two equations above are coupled through the np component and so they must be solved simultaneously. Furthermore, the G -matrix equation and Eqs. (13-14) are coupled through the single-particle energy (which includes the single-particle potential, itself defined in terms of the G -matrix). So we have a coupled system to be solved self-consistently.

Before proceeding with the self-consistency, one needs an *ansatz* for the single-particle potential. The latter is suggested by the most general structure of the nucleon self-energy operator consistent with all symmetry requirements. That is:

$$\mathcal{U}_i(\vec{p}) = U_{S,i}(p) + \gamma_0 U_{V,i}^0(p) - \vec{\gamma} \cdot \vec{p} U_{V,i}(p), \quad (15)$$

where $U_{S,i}$ and $U_{V,i}$ are an attractive scalar field and a repulsive vector field, respectively, with $U_{V,i}^0$ the timelike component of the vector field. These fields are in general density and momentum dependent. We take

$$\mathcal{U}_i(\vec{p}) \approx U_{S,i}(p) + \gamma_0 U_{V,i}^0(p), \quad (16)$$

which amounts to assuming that the spacelike component of the vector field is much smaller than both $U_{S,i}$ and $U_{V,i}^0$. Furthermore, neglecting the momentum dependence of the scalar and vector fields and inserting Eq. (16) in the Dirac equation for neutrons/protons propagating in nuclear matter,

$$(\gamma_\mu p^\mu - m_i - \mathcal{U}_i(\vec{p}))u_i(\vec{p}, \lambda) = 0, \quad (17)$$

naturally leads to rewriting the Dirac equation in the form

$$(\gamma_\mu (p^\mu)^* - m_i^*)u_i(\vec{p}, \lambda) = 0, \quad (18)$$

with positive energy solutions as in Eq. (3), $m_i^* = m + U_{S,i}$, and

$$(p^0)^* = p^0 - U_{V,i}^0(p). \quad (19)$$

The subscript “ i ” signifies that these parameters are different for protons and neutrons.

As in the symmetric matter case [15], evaluating the expectation value of Eq. (16) leads to a parametrization of the single particle potential for protons and neutrons (Eqs.(13-14)) in terms of the constants $U_{S,i}$ and $U_{V,i}^0$ which is given by

$$U_i(p) = \frac{m_i^*}{E_i^*} \langle \vec{p} | \mathcal{U}_i(\vec{p}) | \vec{p} \rangle = \frac{m_i^*}{E_i^*} U_{S,i} + U_{V,i}^0. \quad (20)$$

Also,

$$U_i(p) = \sum_{j=n,p} \sum_{p' \leq k_F^j} G_{ij}(\vec{p}, \vec{p}'), \quad (21)$$

which, along with Eq. (20), allows the self-consistent determination of the single-particle potential as explained below.

The kinetic contribution to the single-particle energy is

$$T_i(p) = \frac{m_i^*}{E_i^*} \langle \vec{p} | \vec{\gamma} \cdot \vec{p} + m | \vec{p} \rangle = \frac{m_i m_i^* + \vec{p}^2}{E_i^*}, \quad (22)$$

and the single-particle energy is

$$e_i^*(p) = T_i(p) + U_i(p) = E_i^* + U_{V,i}^0. \quad (23)$$

The constants m_i^* and

$$U_{0,i} = U_{S,i} + U_{V,i}^0 \quad (24)$$

are convenient to work with as they facilitate the connection with the usual non-relativistic framework [16].

Starting from some initial values of m_i^* and $U_{0,i}$, the G -matrix equation is solved and a first approximation for $U_i(p)$ is obtained by integrating the G -matrix over the appropriate Fermi sea, see Eq. (21). This solution is again parametrized in terms of a new set of constants, determined by fitting the parametrized U_i , Eq. (20), to its values calculated at two momenta, a procedure known as the “reference spectrum approximation”. The iterative procedure is repeated until satisfactory convergence is reached.

Finally, the energy per neutron or proton in nuclear matter is calculated from the average values of the kinetic and potential energies as

$$\bar{e}_i = \frac{1}{A} \langle T_i \rangle + \frac{1}{2A} \langle U_i \rangle - m. \quad (25)$$

The EoS, or energy per nucleon as a function of density, is then written as

$$\bar{e}(\rho_n, \rho_p) = \frac{\rho_n \bar{e}_n + \rho_p \bar{e}_p}{\rho}, \quad (26)$$

or

$$\bar{e}(k_F, \alpha) = \frac{(1 + \alpha) \bar{e}_n + (1 - \alpha) \bar{e}_p}{2}. \quad (27)$$

Clearly, symmetric nuclear matter is obtained as a by-product of the calculation described above by setting $\alpha=0$, whereas $\alpha=1$ corresponds to pure neutron matter.

III. CHIRAL TWO- AND THREE-NUCLEON FORCES

Ideally, one wishes to base a derivation of the nuclear force on QCD. However, the well-known problem with QCD is that it is non-perturbative in the low-energy regime characteristic for nuclear physics. For many years this fact was perceived as a great obstacle to a derivation of nuclear forces from QCD—impossible to overcome except with lattice QCD. The effective field theory concept has shown the way out of this dilemma. One has to realize that the scenario of low-energy QCD is characterized by pions and nucleons interacting via a force governed by spontaneously broken approximate chiral symmetry. This chiral EFT allows for a systematic low-momentum expansion known as chiral perturbation theory (ChPT). Contributions are analyzed in terms of powers of small external momenta over the large scale, $(Q/\Lambda_\chi)^\nu$, where Q is generic for an external momentum (nucleon three-momentum or pion four-momentum) or pion mass, and $\Lambda_\chi \approx 1$ GeV is the chiral symmetry breaking scale (‘hard scale’). (See Ref. [7] and references therein.)

The past fifteen years have seen great progress in applying ChPT to nuclear forces. As a result, NN potentials of high precision have been constructed, which are based on ChPT carried to next-to-next-to-next-to-leading order (N³LO). We will apply here the chiral NN potential of Ref. [9] which uses a cutoff, Λ , equal to 500 MeV.

A great advantage of the EFT approach to nuclear forces is that it creates two- and many-body forces on an equal footing. Three-nucleon forces make their appearance at the third order in the chiral power counting. These leading-order contributions are: the long-range two-pion exchange graph; the medium-range one-pion exchange diagram; and the short-range contact term.

In Ref. [17], density-dependent corrections to the in-medium NN interaction have been derived from the leading-order chiral 3NF. These are effective two-nucleon interactions that reflect the underlying three-nucleon forces and are therefore computationally very convenient, whereas realistic models of three-nucleon forces would be prohibitive.

A total of six one-loop diagrams contribute at this order. Three are generated by the two-pion exchange graph of the chiral three-nucleon interaction and depend on the low-energy constants $c_{1,3,4}$, which are fixed in the NN system [9]. We use $c_1 = -0.81$ GeV⁻¹, $c_3 = -3.2$ GeV⁻¹, and $c_4 = 5.4$ GeV⁻¹. Two are generated by the one-pion exchange diagram and depend on the low-energy constant c_D . Finally, the short-range component depends on the constant c_E . The constants c_D and c_E can be fixed by fitting properties of few-nucleon systems, such as the triton and ³He binding energies [18]. We use $c_D = 5.0$ and $c_E = 0.48$.

In pure neutron matter, the contributions proportional to the low-energy constants c_4 , c_D , and c_E vanish [17]. Analytical expressions for these corrections are provided in Ref. [17] in terms of the well-known non-relativistic two-body nuclear force operators. These can be conveniently incorporated in the usual NN partial wave formalism and the conventional BHF theory.

IV. RESULTS

In Fig. 3, we display the EoS of SNM obtained with the two approaches outlined above. The (blue) solid lines denote the results from the meson-exchange Bonn potential and the conventional BHF approximation (“BnB BHF”) or the relativistic DBHF (“BnB DBHF”), while the chiral calculations are shown by the (red) dashed lines, with and without 3NF, as denoted.

As to be expected, both the conventional BHF calculation and the one using only the two-body chiral potential N³LO display excessive attraction and are unable to produce saturation up to very high density. The “Dirac effect” brings in a powerful saturation mechanism as seen by comparing the two (blue) solid curves. A very similar effect, both qualitatively and quantitatively, is generated by the effective chiral 3NF.

In spite of the differences between the two approaches, the predictions are very close, not only in the value of the energy at saturation, but also the density dependence of the saturation mechanism. We notice, though, that the DBHF energies tend to grow faster at the higher densities.

The same comparison is done in Fig. 4 for neutron matter, yielding similar conclusions. Here, too, the DBHF energies show a faster growth as density increases.

In Fig. 5, we display the symmetry energy as obtained with the well-known parabolic approximation, $e_{sym} = e_{NM} - e_{SNM}$. (Notice that at this point we only consider the versions of the BnB- and the N³LO-based calculations which have realistic saturation properties, see Fig. 3.)

The slope of the symmetry energy, usually defined in terms of the L parameter, ($L = 3\rho_0(\frac{de_{sym}}{d\rho})_{\rho_0}$), is a measure of the pressure gradient between neutron and symmetric matter. A variety of experiments are aimed at constraining this important quantity [1], which correlates nearly linearly with the neutron skin of neutron-rich nuclei. At the present time there seems to be a consensus from various experiments that the acceptable range of values of the symmetry energy and its slope at saturation are centered around e_{sym} and L equal to 32.5 MeV and 70 MeV, respectively [1]. The values of the L parameter obtained with “BnB+DBHF” and “N³LO+3NF” are 69 and 61 MeV, respectively.

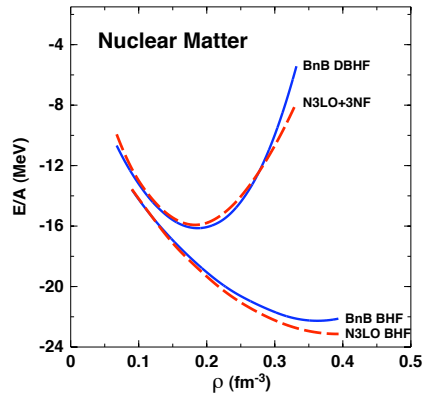


FIG. 3: Energy/particle in SNM. The solid (blue) lines are obtained with Bonn B + DBHF (upper curve) and Bonn B + BHF (lower curve). The dashed (red) lines show the predictions by the $N^3\text{LO}$ potential with (upper curve) and without (lower curve) chiral three-nucleon forces.

Notice that the typical uncertainty on the L parameter is as large as 20-25 MeV [1].

How the differences/similarities noted above impact neutron star bulk properties is examined in Fig. 6. (Since our focal point is a comparison between two theoretical approaches, rather than a detailed calculation of β -stable matter composition, we consider only neutron stars made of pure neutron matter.) We also note that, in order to extend the chiral predictions to the high densities probed by compact stars, we fit a three-parameter function, $e(\rho) = \alpha\rho + \beta\rho^\gamma$, to the “ $N^3\text{LO}+3\text{NF}$ ” predictions of Fig. 4 and use this *ansatz* to obtain the high-density EoS needed for neutron star calculations.

The comparison in Fig. 6 shows a larger star maximum mass for “BnB DBHF”, most likely the result of larger repulsion of that model at high density. Overall, the predicted star bulk properties are only moderately different in the two approaches.

V. CONCLUSIONS

We have considered two very different methods to approach the study of nucleonic matter: one based on a meson-theoretic potential and the Dirac-Brueckner-Hartree-Fock approximation; the other based on a high-precision chiral NN potential and chiral effective three-nucleon forces at NNLO. The predictions we have considered include: the EoS of nuclear and neutron matter, the symmetry energy and its slope, and the mass-radius relation in a neutron star.

From our results, we conclude that the DBHF method is an excellent phenomenology capable of incorporating important many-body effects that are crucial to nuclear saturation.

In both approaches, the effective 3NF is generated by one nucleon interacting with the Fermi sea. That is, in both cases we have effective two-nucleon interactions that reflect the underlying three-nucleon forces. No matter if this interaction proceeds *via* relativistic meson exchange or *via* chiral EFT forces, the results are very similar. This is reassuring and confirms that the two ways of describing nuclear forces are complementary.

Acknowledgments

Support from the U.S. Department of Energy under Grant No. DE-FG02-03ER41270 is acknowledged, and from the Italian Ministero dell’Istruzione dell’Università della Ricerca (MIUR) under PRIN 2009. We are grateful to F.

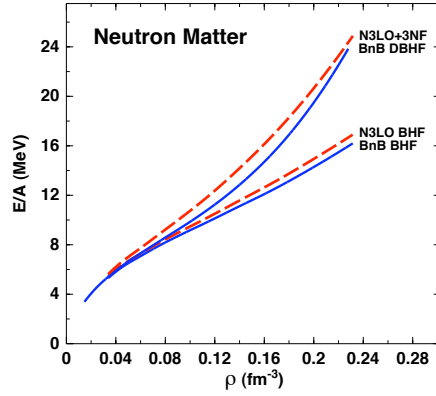


FIG. 4: Same as Fig. 3, but for neutron matter.

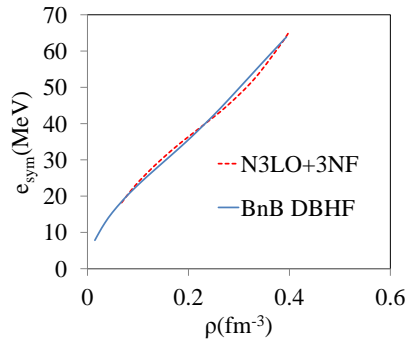


FIG. 5: The symmetry energy *vs.* density for the models corresponding to the two upper curves in Fig. 3-4.

Weber for providing his TOV code for the calculation of neutron star properties.

-
- [1] M.B. Tsang *et al.*, *Phys. Rev. C* **86**, 015803 (2012).
 - [2] F. Sammarruca, *Int. J. Mod. Phys. E*, **19**, 1259 (2010).
 - [3] S. Weinberg, *Phys. Rev.* **166**, 1568 (1968).
 - [4] G.E. Brown, in *Mesons in Nuclei*, eds. M. Rho and D.H. Wilkinson, Vol. I (North-Holland, Amsterdam, 1979), 330.
 - [5] Z.H. Li, U. Lombardo, H.-J. Schulze, and W. Zuo, *Phys. Rev. C* **77**, 034316 (2008).
 - [6] S. Weinberg, *Physica* **96A**, 327 (1979).
 - [7] R. Machleidt and D.R. Entem, *Phys. Rep.* **503**, 1 (2011).
 - [8] R. Machleidt, *Adv. Nucl. Phys.* **19**, 189 (1989).

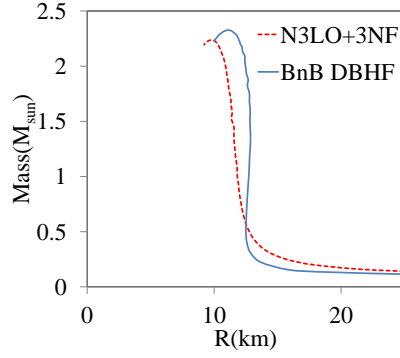


FIG. 6: Neutron star mass-radius relation as predicted by the two models as denoted.

- [9] D.R. Entem and R. Machleidt, *Phys. Rev. C* **68**, 041001 (2003).
- [10] R. Machleidt, *Phys. Rev. C* **63**, 024001 (2001).
- [11] V.G.J. Stoks *et al.*, *Phys. Rev. C* **49**, 2950 (1994).
- [12] R.H. Thompson, *Phys. Rev. D* **1**, 110 (1970).
- [13] E.E. Salpeter and H.A. Bethe, *Phys. Rev.* **84**, 1232 (1951).
- [14] D. Alonso and F. Sammarruca, *Phys. Rev. C* **67**, 054301 (2003).
- [15] R. Brockmann and R. Machleidt, *Phys. Lett. B* **149**, 283 (1984); *Phys. Rev. C* **42**, 1965 (1990).
- [16] M.I. Haftel and F. Tabakin, *Nucl. Phys.* **A158**, 1 (1970).
- [17] J.W. Holt, N. Keiser, and W. Weise, *Phys. Rev. C* **81**, 024002 (2010).
- [18] P. Navratil, V.G. Gueorguiev, J.P. Vary, W.E. Ormand, and A. Nogga, *Phys. Rev. Lett.* **99**, 042501 (2007).